7 November 1994

PHYSICS LETTERS A

ELSEVIER

Physics Letters A 194 (1994) 289–294

Bifurcations of a three-torus in a twin-stripe semiconductor laser model

Ortwin Hess [a], Detlef Merbach [b], Hans-Peter Herzel [b], Eckehard Schöll [b]

[a] *Fachbereich Physik, AG Halbleiterphysik, Philipps-Universität Marburg, Renthof 5, D-35032 Marburg/Lahn, Germany*
[b] *Institut für Theoretische Physik, Technische Universität Berlin, Hardenbergstrasse 36, D-10623 Berlin, Germany*

Received 18 April 1994; revised manuscript received 7 September 1994; accepted for publication 7 September 1994
Communicated by A.P. Fordy

Abstract

The dynamic behaviour of the strongly coupled twin-stripe semiconductor laser is studied theoretically in dependence on the pumping strength (current injection). With the aid of power spectra, next-maximum maps, and estimates of the attractor dimensions bifurcations from a three-torus to a two-torus and from two-tori to chaotic attractors are identified.

1. Introduction

Frequently, the dynamics of arrays of coupled lasers has been modelled by discrete coupled nonlinear oscillators [1–3], involving ordinary differential equations. In this paper, we analyze the dynamics of the twin-stripe semiconductor laser based on a system of phenomenological partial differential equations allowing for a continuous description of the transverse optical pattern [4–6]. In previous numerical simulations based on this model it has been observed that the twin-stripe laser may exhibit three dynamical regimes [6], depending on the separation between the laser stripes: (i) For separation $s \approx 5$ μm the lasers are strongly coupled and show tori and low-dimensional chaos. (ii) With increasing stripe separation the correlations between the two stripes gradually become weaker and more complex spatio-temporal behaviour indicative of higher dimensional chaos is observed. (iii) At a certain critical maximum stripe separation the two stripes start to behave as individual lasers, each of which exhibits the typical relaxation oscillations of single-stripe semiconductor lasers.

The focus of our attention in this paper is the strongly coupled twin-stripe laser (i) where the separation between the two laser stripes is of the order of the diffusion length of the charge carriers. We will concentrate on analyzing its dynamics with methods of time-series analysis. There, as will be shown in the following, the variation of the pumping-strength, i.e., the injection current, has tremendous influence on the dynamics.

2. Modelling spatio-temporal dynamics

The dynamics of the longitudinally (in the z-direction, cf. Fig. 1) slowly varying counterpropagating optical fields $E^{\pm}$ and the dynamics of the electron–hole density N are described by a model system of coupled nonlinear partial differential equations [4–6]. In the following simulation (with the exception of Fig. 2) we use a mean-field approximation [7] for the longitudinally averaged field $E = \overline{E^+} = \overline{E^-}$,

SSDI 0375-9601(94)00733-0

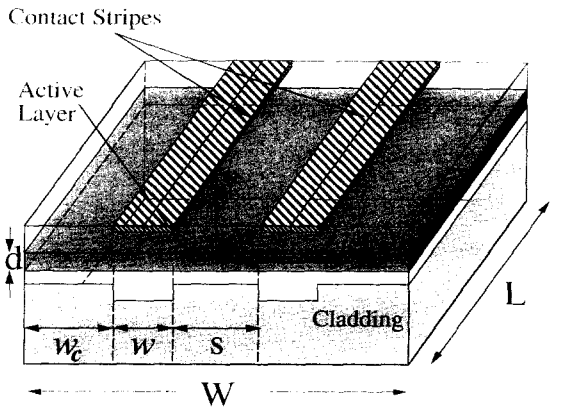

Fig. 1. Schematic structure of a combined gain- and index-guided GaAs/$Al_xGa_{1-x}As$ twin-stripe laser.

$$\frac{n_l}{c}\frac{\partial E}{\partial t} = iD_p\frac{\partial^2 E}{\partial x^2} - [\gamma_m + i\eta(x)]E + \Gamma(x)[g(N) - i\alpha a N]E, \quad (1)$$

$$\frac{\partial N}{\partial t} = A(x) + D_f\frac{\partial^2 N}{\partial x^2} - \frac{N}{\tau} - 2g(N)|E|^2 \quad (2)$$

The optical gain and the change of the refractive index of the active medium are modeled by the phenomenological linear gain-function $g(N) = a(N - N_0)$ and $\delta n = -\alpha a N/k_0$, respectively [8], where the differential gain is $a = 1.5\times10^{-16}\mathrm{cm}^2$, $N_0 = 0.64\times10^{18}\mathrm{cm}^{-3}$ is the carrier density at transparency, $n_l = 3.59$ is the refractive index of the active semiconductor layer, $k_0 = 2\pi/\lambda$ is the wavenumber in vacuum, $\lambda = 815$ nm the optical wavelength, c the speed of light and ε_0 is the vacuum permittivity. The linewidth enhancement or anti-guiding factor $\alpha = 2$ is assumed as constant. Spatial and temporal variations of α which become important, e.g., in broad-area semiconductor lasers [9,10] are thus disregarded.

The non-radiative decay of the electron–hole density is represented by the recombination time $\tau = 5$ ns. The diffraction coefficient $D_p = (2n_l k_0)^{-1} = 18\times10^{-6}$ m results from the paraxial ray approximation [11] which has been performed to obtain (1) from Maxwell's equations [4]. The transverse passive waveguiding properties are characterized by $\eta(x) = k_0(n_c - n_{\mathrm{eff}})$ for $x_i - w/2 \leqslant x \leqslant x_i + w/2$ and $\eta(x) = k_0 n_c$ in the regions between the stripes, where x_i, $i = 1, 2$, is the center of the ith laser, $w = 5$ μm its width, $n_{\mathrm{eff}} = 3.42$ its effective index, and $n_c = 3.35$ is the refractive index of the cladding layer. The confinement factor $\Gamma(x) = 0.5149$ for $x_i - w/2 \leqslant x \leqslant x_i + w/2$, and $\Gamma(x) = 0.5013$ between the laser stripes, represents the transverse dependence of the vertical confinement of the optical field to the active layer. The distributed loss at the facets is represented by the parameter $\gamma_m = \ln\sqrt{R_1R_2}/2L$, where $R_1 = 0.32$ and $R_2 = 0.99$ are the reflectivities of the facet mirrors at $z = 0$ and $z = L = 250$ μm, respectively. The *transverse* boundary conditions $\partial E/\partial x = -\alpha_w E, \partial N/\partial x = -\alpha_{sr}N$ at $x = +W/2$ and $\partial E/\partial x = +\alpha_w E, \partial N/\partial x = +\alpha_{sr}N$, at $x = -W/2$ where $W = s + 2w + 2w_c$, with s being the stripe separation, account for the absorption ($\alpha_w = 30$ cm^{-1}) in the "wings" ($w_c = 10$ μm) outside the laser stripes, and the charge carrier recombination effects (α_{sr}) at the surface of the structure. The surface-recombination coefficient [12] $\alpha_{sr} = v_{sr}/D_f$

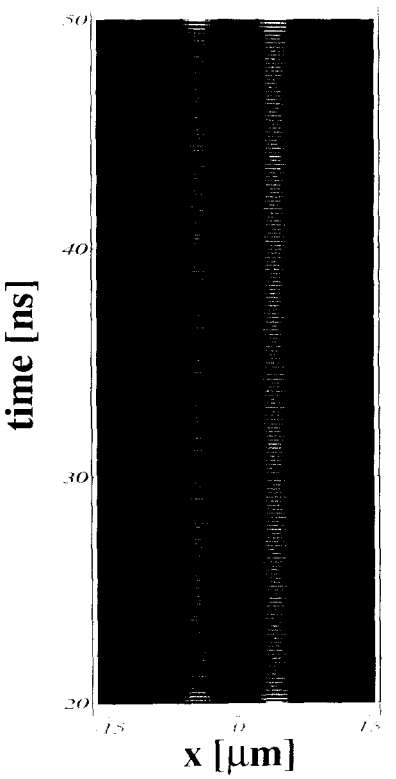

Fig. 2. Computed near-field intensity $I(x,t)$ for the strongly coupled twin-stripe semiconductor laser with a stripe separation of $s = 5$ μm and an injection current $I = 50$ mA per laser stripe. Bright colors represent high light intensity, dark shading indicates low intensity values.

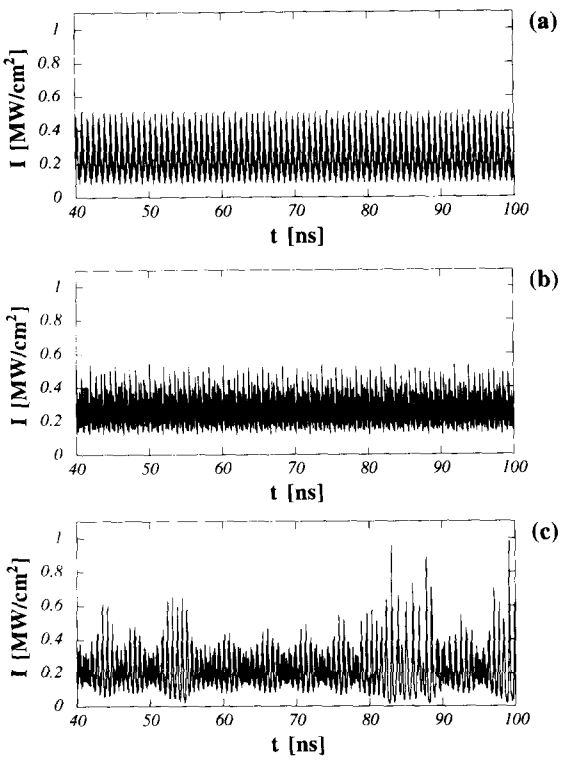

Fig. 3. Three typical examples of the time-series $I(t)$ obtained by transverse spatial averaging from the simulated spatio-temporal intensity distribution for $s = 5.5\,\mu$m and different injection currents J. (a) $J = 47$ mA, (b) $J = 51$ mA, and (c) $J = 45$ mA.

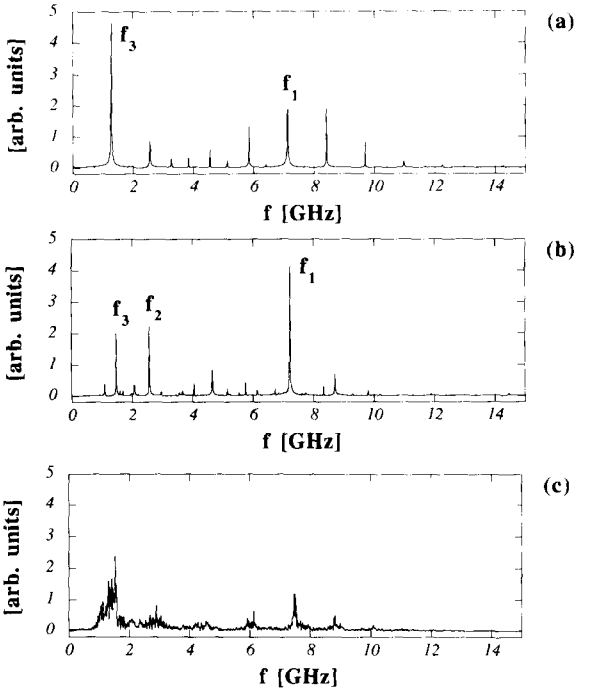

Fig. 4. Power spectra of the time series in Fig. 3. (a) $J = 47$ mA, (b) $J = 51$ mA, and (c) $J = 45$ mA.

includes the diffusion coefficient $D_f = 30$ cm^2/s and the surface recombination velocity $v_{sr} = 10^6$ m/s. The coupled system of nonlinear partial differential equations (1), (2) is discretized in time (t) and space (x, z) and the resulting finite-difference equations are integrated using the *Hopscotch* method [5,13].

The transversely dependent excitation of the two oscillators – determined by the injection of charge carriers through the two contact stripes (hatched in Fig. 1) at the top of the device – is applied at $t = 0$ with a step-function and held constant in time. It is represented by the pumping term $\Lambda(x) = j\eta_i/ed$ for $x_i - w/2 \leqslant x \leqslant x_i + w/2$ and $\Lambda(x) = 0$ otherwise. The injection current density is denoted by j, $\eta_i = 1$ representing the injection efficiency has been assumed, e is the electron charge and $d = 0.15\,\mu$m the (vertical) thickness of the layer.

Fig. 2 shows as an example the dynamics of the output intensity at the front facet $I(x,t) = T_1|E(x,t)|^2/Z$, $Z = n_l/\varepsilon_0 c$ and $T_1 = 1 - R_1$ being the optical wave-resistance in the semiconductor medium and the transmittivity of the front mirror, respectively. The separation $s = 5\ \mu$m between the two laser stripes is within the typical diffusion length of the change carriers which are injected through the two current stripes on the top of the laser. In the following, however, we will concentrate on the analysis of the dynamics of the transversely averaged optical intensity – as frequently done in experiments – and vary the injection current $J = jwL$ which is applied to the twin-stripe laser. Note that in spite of this averaging the consideration of the spatial dimension in the simulation is vital. It has been shown [14] using empirical orthogonal functions that the bifurcations discussed below are accompanied by qualitative changes of the spatio-temporal patterns. However, in this paper we focus on the temporal dynamics.

3. Dynamics and bifurcations

In Fig. 3 we have plotted the transversely averaged optical intensity $I(t)$ for three different injection currents. The time series in Fig. 3a ($J = 47$ mA) shows

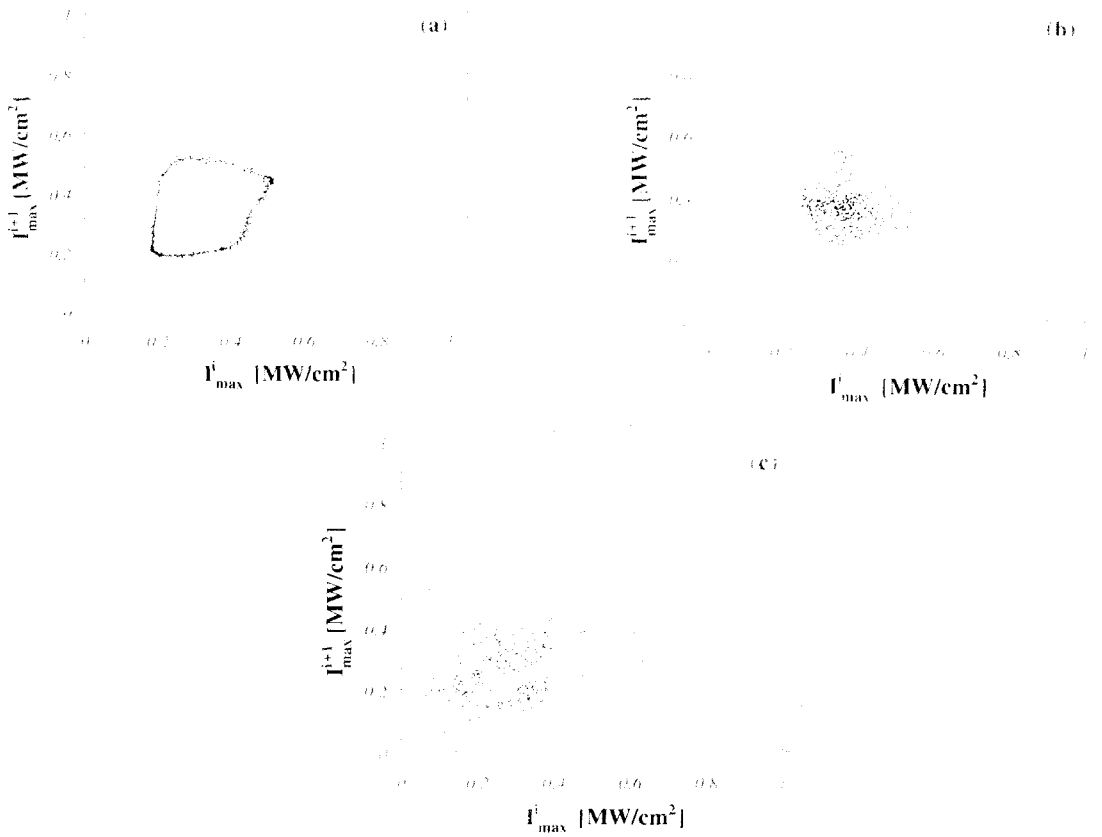

Fig. 5. Map of consecutive maxima of the spatially averaged intensity. (a) $J = 47$ mA, (b) $J = 51$ mA, and (c) $J = 45$ mA.

oscillations with varying amplitudes. More information than by mere visual inspection can be obtained from a Fourier transform of the time series. In the corresponding power spectrum, where data from the interval from 40 to 100 ns have been used, the frequency peaks in Fig. 4a can be explained by linear combinations of two incommensurate fundamental frequencies f_1 and f_3, suggesting dynamics on a two-torus. The frequency peaks in Fig. 4b, corresponding to the time series in Fig. 3b, however, cannot be explained by two frequencies alone. Careful analysis of the spectrum reveals that more than 15 peaks can be explained as a superposition of three incommensurate frequencies f_1, f_2, and f_3. Hence, a three-torus is indicated. According to theorems by Ruelle, Takens, and Newhouse [15,16] such three-tori are not generic and, consequently, small variations of parameters should give frequency locking or strange attractors [17]. Indeed, the spectrum in Fig. 4c, corresponding to the time series of Fig. 3c, is profoundly different from the spectra in Figs. 4a and 4b, and indicates chaotic dynamical behaviour.

We emphasize that our simulations involve a large number of spatial degrees of freedom, and the possibility of artificially generated "numerical noise" due to the discretization procedure cannot be a priori excluded. Therefore in the following we apply several methods of time-series analysis to substantiate our hypothesis that the dynamics can be interpreted in terms of bifurcations from a three-torus to a two-torus or to a chaotic attractor.

At first we consider maps of consecutive maxima of the intensity which are topologically equivalent to Poincaré sections of the dynamic flow. Fig. 5a, corresponding to the injection current $J = 47$ mA, suggests indeed that the dynamics of the twin-stripe laser is

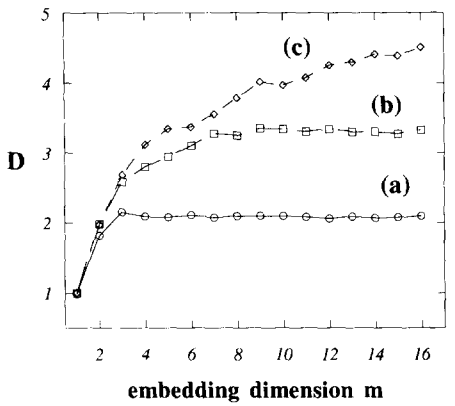

Fig. 6. Near-neighbour dimension D versus embedding dimension m. Time delay $\tau = 52.3$ ps, neighbour order $k = 100$. (a) $J = 47$ mA, (b) $J = 51$ mA, and (c) $J = 45$ mA.

confined to a two-torus. The plots in Figs. 5b and 5c indicate higher dimensional attractors. For the proposed three-torus (Fig. 5b), the points are more strongly confined distributed than for the chaotic time-series (Fig. 5c) which gives a hint of the difference between both situations.

In order to analyze the attractors quantitatively we have estimated the corresponding fractal dimensions using a nearest neighbour algorithm [1] [18,19]. It is based on the calculation of the distances d_k in a reconstructed pseudo-phase space between attractor points and their kth neighbour. Denoting the number of points chosen for the calculation of the mean distance $\langle d_k \rangle$ by N, it was shown that $\langle d_k \rangle$ scales $\sim N^{-1/D}$. We have carefully checked the dependence of the estimated dimension D on the parameters of the phase space reconstruction (embedding dimension m, delay time τ) and on the order k of the neighbours. It turned out that the number of available data points $N_{\text{tot}} = 8192$ is sufficient to get reasonable estimates for $D \leqslant 3$. Fig. 6 displays the dependence of the estimate of D on the embedding dimension m. The convergence of D in curves (a) and (b) of Fig. 6 to values around 2 and 3, respectively, is consistent with the results in our previous analysis. The chaotic time series (Fig. 3c) does not show such a saturation at integer values. Hence, with the available number of data points the dimension cannot be determined quantitatively.

[1] We used an implementation by E. Kostelich.

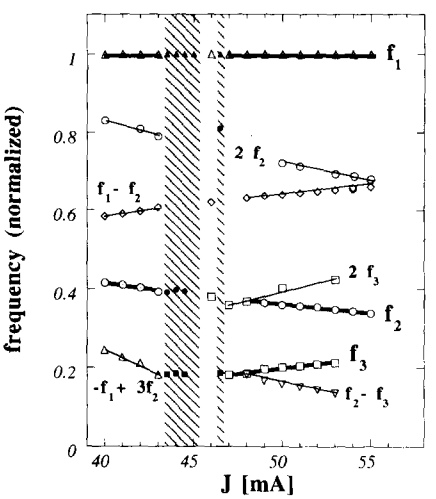

Fig. 7. Frequency bifurcation diagram. The normalized frequencies and their linear combinations are plotted as a function of the injection current J. The bold lines denote incommensurate frequencies. The hatched areas mark the chaotic regimes.

So far we have analyzed three representative time-series for injection currents $J = 45$, 47, and 51 mA. It turned out that the dynamics is governed by the interaction of three frequencies. In order to get a systematic overview of the bifurcations due to varying current we have plotted in Fig. 7 the dominant frequency peaks as a function of J. For convenience, the frequencies are normalized to f_1 which is in the order of 8 GHz.

Besides the frequencies f_2 and f_3 also the harmonics $2f_2$, $2f_3$ and the linear combinations $f_1 - f_2$, $f_2 - f_3$ and $-f_1 + 3f_2$ are clearly visible. Note, that the three fundamental frequencies are incommensurate only in those regimes where they are marked by bold solid lines, i.e., a three-torus is found only where three solid lines coexist. Thus, with increasing J, a two-torus, a chaotic band with a quasiperiodic window, a two-torus, and a three-torus, subsequently appear. A bifurcation from the two-torus to a chaotic attractor occurs at $J \approx 43.5$ mA. With decreasing J, frequency locking from the three-torus to the two-torus happens at $J \approx 48$ mA, where $f_2 = 2f_3$, and the two-torus eventually breaks up into a chaotic attractor at $J \approx 46.6$ mA. In the two chaotic regions (hatched) there still exist frequency peaks in the broad-band noise underground which fit into the global scheme.

4. Discussion

We have analyzed the dynamical behaviour of the strongly coupled twin-stripe laser and observed bifurcations in the time dependence of the spatially averaged output intensity between quasiperiodic and chaotic attractors upon variation of the applied injection current. By calculating the power spectra of the time series, next-maximum maps, nearest-neighbour dimensions and, in particular, by a detailed analysis of the peaks of the spectrum, bifurcations between two- and three-tori and temporally chaotic behaviour are identified.

Motivated by the theoretical considerations of Ruelle, Takens, and Newhouse, Grebogi et al. have studied in detail bifurcations from N-tori [17]. In their numerical work they found that at parameters adjacent to a three-torus in most cases two-tori and, to a lesser extent, limit cycles and strange attractors appear. Our results can be regarded as an exemplification of such a destruction of three-tori.

The underlying physical mechanisms of the generation of a second and third frequency are not yet clear. It is worth mentioning that for stripe separations $s < 5\ \mu$m the oscillations are symmetric with respect to stripes 1 and 2 and with increasing distances between the stripes the appearence of complex dynamics around $s = 5\ \mu$m is preceded by a breaking of the symmetry. Although the structure of the twin-stripe laser is symmetric, in all our simulations reported above one of the stripes had a higher mean intensity than the other one. By choosing other initial conditions the corresponding mirror-image of this asymmetric attractor can be selected.

In conclusion, we emphasize that semiconductor laser arrays, which are technologically important devices, appear to offer interesting applications of theoretical concepts from nonlinear dynamics.

Acknowledgement

O.H. wants to thank I. Fischer, M. Sauer and J. Lenonardi for valuable and interesting discussions. Partial financial support from the Deutsche Forschungsgemeinschaft is gratefully acknowledged.

References

[1] H.G. Winful and L. Rahman, Phys. Rev. Lett. 65 (1990) 1575.
[2] K.A. Shore, SPIE 667 (1986) 109.
[3] T.E. Rozzi and K.A. Shore, J. Opt. Soc. Am. B 2 (1985) 237.
[4] H. Adachihara, O. Hess, R. Indik and J.V. Moloney, J. Opt. Soc. Am. B 10 (1993) 496.
[5] O. Hess, Spatio-temporal dynamics of semiconductor lasers (Wissenschaft und Technik Verlag, Berlin, 1993).
[6] O. Hess and E. Schöll, Physica D 70 (1994) 165.
[7] L.A. Lugiato, Theory of optical bistability, in: Progress in optics, Vol. 21, ed. E. Wolf (North-Holland, Amsterdam, 1984) p. 71.
[8] G.P. Agrawal and N.K. Dutta, Long-wavelength semiconductor lasers (Van Nostrand Reinhold, New York, 1986).
[9] H. Adachihara, O. Hess, E. Abraham, P. Ru and J.V. Moloney, J. Opt. Soc. Am. B 10 (1993) 658.
[10] O. Hess, Spatio-temporal complexity in multi-stripe and broad-area semiconductor lasers, invited contribution to Chaos, Solitons, and Fractals, special issue on Transverse nonlinear optics, ed. L. Lugiato, to be published.
[11] M. Lax, W.H. Louisell and W. B McKnight, Phys. Rev. A 11 (1975) 1365.
[12] K. Tai, T.R. Hayes, S.L. McCall and W.T. Tsang, Appl. Phys. Lett. 53 (1988) 302.
[13] I.S. Grieg and J.D. Morris, J. Comput. Phys. 20 (1976) 60.
[14] O. Hess and E. Schöll, Eigenmodes of the dynamically coupled twin-stripe semiconductor laser, Phys. Rev. A 50 (1994) 787.
[15] D. Ruelle and F. Takens, Commun. Math. Phys. 20 (1971) 167.
[16] S. Newhouse, D. Ruelle and F. Takens, Commun. Math. Phys. 64 (1978) 35.
[17] C. Grebogi, E. Ott and J.A. Yorke, Physica D 15 (1985) 354.
[18] R. Badii and A. Politi, J. Stat. Phys. 40 (1985) 725.
[19] W. Mende, H. Herzel and K. Wermke, Phys. Lett. A 149 (1990) 418.